Surface Review and Letters, 2150055 (7 pages)

DOI: 10.1142/S0218625X21500554

World Scientific
www.worldscientific.com

REFLECTANT PHOTONIC CRYSTALS PRODUCED VIA POROUS-ALUMINA-ASSISTED-ANODIZING OF Al/Nb AND Al/Ta SYSTEMS

ANDREI PLIGOVKA*
Research and Development Laboratory 4.10 "Nanotechnologies",
Belarusian State University of Informatics and Radioelectronics,
Brovki Str. 6, Minsk 220013,
The Republic of Belarus
**pligovka@bsuir.by*

Received 15 July 2020
Revised 13 March 2021
Accepted 14 March 2021
Published 6 May 2021

The development of new nanomaterials with controlled characteristics for nanophotonics is of great relevance. In this work, photonic crystals with reflectance at the wavelength of 690 nm and the value of 28% were formed by porous-alumina-assisted-anodizing of system Al/Ta on Si wafer. By selecting improved anodizing modes of system Al/Nb on glass, the reflectance was increased to 42% at the wavelength of 340 nm. This result shows the high promise of the proposed methods and in the future will significantly improve the result by trying two- or three-stage methods of porous-alumina-assisted-anodizing, nanoimprint stamps and optimization of the anodizing modes for any wavelengths.

Keywords: Tantalum oxide; niobium oxide; porous anodic alumina; optical reflectance; nanostructured materials; anodization; anodic aluminum oxide.

1. Introduction

Tantalum- and niobium-oxides are promising materials for optics and photonics.[1–5] In work Ref. 6, photonic crystals (PCs) waveguide structures were fabricated in Ta_2O_5 on SiO_2 by means of e-beam lithography and electron cyclotron resonance etching. Tantalum pentoxide has the refractive index of 2.08 at the optical wavelength of $\lambda = 1550$ nm. The PCs devices were fabricated and investigated in Ref. 6 by various submicron high aspect ratio air hole patterns with typical hole diameters of 280–400 nm and the depth of 1.5 nm. It was shown that the optical properties of the fabricated PCs structures are strongly dependent on their geometrical parameters. In the paper Ref. 7, a silica opal was infiltrated by tantalum (V) ethoxide to deposit Ta_2O_5 using a metal-organic chemical vapor deposition process. The obtained inverse opal showed a strong reflectance in the UV-range (~350 nm) due to the small lattice parameter of the crystal and the high refractive index of Ta_2O_5. The control of this UV-reflectance is a step towards the full photonic bandgap in the UV-Visible which is currently the main challenge in this field. Fabrication and characterization of Ta_2O_5 photonic feedback structures were presented in Ref. 8. The work demonstrates that photonic feedback structures from

Ta_2O_5 offer great potential for the fabrication of organic laser devices in the visible wavelength range. They are a viable alternative to structured TiO_2 with easier processing and low optical losses.

Bandgap energy of niobium-oxide is 3.4 eV,[9,10] the value close to that of TiO_2 (about 3.2 eV Ref. 11) and is, therefore, suitable for the use as a photocatalyst under UV-light.[5] The work Ref. 12 presents the results of the formation of PCs with high reflectance within photonic bandgap based on porous anodic titania. The optimization of anodizing parameters allowed us to prepare anodic titanium oxide PCs with reflectance within the photonic bandgap of up to 85%. It can be noted that the methods of forming PCs by porous-alumina-assisted-anodizing are very promising due to the efficiency and high control of morphological parameters through electrochemical modes. As known, a PC is a structure with periodically changing layers with low and high refractive indexes, and niobium-oxide like tantalum-oxide has one of the highest refractive indexes.

Summing up, it can be noted that tantalum- and niobium-oxides are highly promising for the use in nanophotonics as PCs. However, nowadays economical and at the same time effective methods of structuring these materials under the ultraviolet and visible wavelengths have not been presented yet.

In this work, two different types of PCs on different substrates were formed by porous-alumina-assisted-anodizing and their reflectance in UV-VIS-NIR ranges was measured.

2. Experimental Methods

2.1. *Sample preparation*

PCs were formed from bilayer Al/Nb (1000/50 nm) and Al/Ta (1500/500 nm) systems by magnetron sputter-deposition on rectangular $6 \times 9\,cm^2$ polished glass of 1070 μm thickness and on 100 mm Si wafer (n-type, 4", 500 μm thick, 4–40 $\Omega \cdot$ cm), respectively. Substrates were cut into pieces with $6\,cm^2$ area and anodized in specially designed cylindrical two-electrode cell made of polytetrafluoroethylene (PTFE) to take account of the design features of spectrophotometric analysis and exception meniscus effect in the anodizing process. The anodizing cell consists of an electrolyte bath with a built-in anode, which is screwed into a base and presses the 22 mm Si or glass piece to the ceramic insert by a PTFE ring. The cathode is made of stainless metal located in the electrolyte. Si (glass) piece is individually introduced in the anodizing cell, was pressed from face sides by a PTFE ring, so that a circular area of the face side of the Si (glass) piece, 19 mm in diameter — $2.83\,cm^2$, was in contact with anodizing solution while the back Si (glass) piece side was fully isolated from the processing. A Keysight N5751A programmable power supply controlled by LabVIEW software via laptop and a general-purpose interface bus cable was used as the anodizing unit. After the anodizing and re-anodizing processes, the sample was rinsed in running distilled water for 10 min and dried in warm air for 5 min.

The forming processes of the anodic PCs are outlined in Fig. 1. The PCs were formed by porous-alumina-assisted-anodizing the Al/Nb pieces on glass in $0.2\,mol \cdot dm^{-3}$ oxalic acid aqueous solution at 53 V and Al/Ta pieces on Si wafer [Fig. 1(a)] in $0.2\,mol \cdot dm^{-3}$ tartaric acid aqueous solution at 200 V, until the aluminum metal was fully oxidized as displayed in Fig. 1(b). Then the process was supported into a voltage-stabilization mode, at which the current began to decay. During this step, the alumina barrier layer touches the niobium as shown in Fig. 1(c), local oxidation occurs through the alumina pores and continues until the array of embryo is formed at the interface. Next samples were porous-alumina-assisted high-voltage re-anodizing in the mixed solution of $0.5\,mol \cdot dm^{-3}$ boric acid and $0.05\,mol \cdot dm^{-3}$ sodium tetraborate in potentiodynamic mode at increase potential until the voltage of 230 V for niobium-oxide nanocolumns and 400 V for tantalum-columns was reached. Re-anodizing current was maintained in 300 μA per cm^2 region. Based on the previous results,[13,14] the thickness of niobium film was selected so that after re-anodizing it was completely oxidized. This is possible due to the ability of a niobium continuous layer NbO_2 to conduct electric current as shown in the works[15] in contrast to a continuous layer of tantalum-oxide which is dielectric.[16] The PCs based on tantalum-oxide nanocolumns were formed on an opaque Si-wafer with a 500 nm thick tantalum underlayer. The anodizing conditions were such that a continuous consolidation layer under the tantalum-oxide columns was not formed. The porous-alumina-cell size was too large. During each anodization process, the temperature

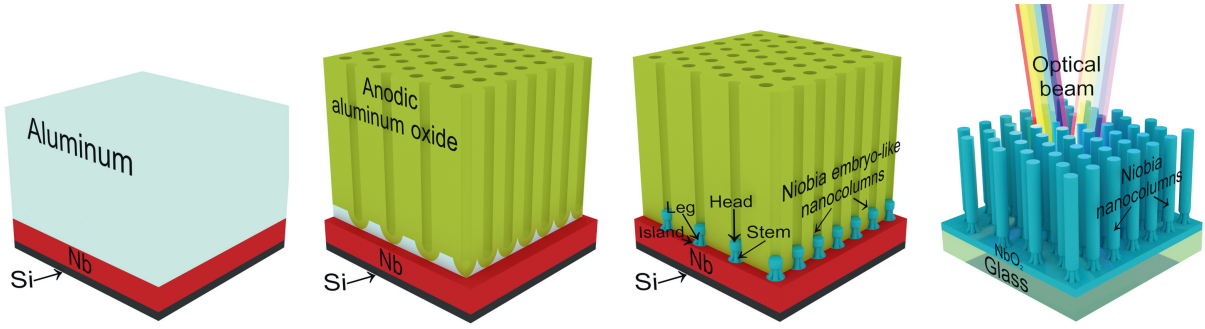

(a) (b) (c) (d)

Fig. 1. Schematic diagram showing the main steps for forming niobium- and tantalum-oxide PCs via porous-alumina-assisted-anodizing of systems Al/Nb and Al/Ta on Si wafer and glass: (a) sputter-deposition of Al/Nb (Ta) bilayer; (b) anodizing the Al layer to form porous-alumina film; (c) porous-alumina-assisted-anodizing of the Nb (Ta) layer; (d) porous-alumina-assisted high-voltage re-anodizing of the Nb (Ta) layer on glass substrate to grow niobium-oxide nanocolumns after removal porous-alumina and incidence scheme of the reflectant optical beam on the experimental sample.

was maintained as constant as possible, typically within +1°C of the set value. To remove porous-alumina aqueous solution of 50% phosphoric acid at 50°C within 30 min was used.

2.2. *SEM observations and optical measurement*

PCs morphology was investigated by scanning electron microscopy (SEM) in a Hitachi S-4800 operated at 10–15 kV. A gold layer, about 4 nm in thickness, was evaporated over the specimens to reduce the charging effects. The metrological certification of Hitachi S-4800 showed exactly geometric dimensions about 7%. The experimental results outlined in papers Refs. 17 and 18 strongly suggest that the SEM can be used to make accurate overlay measurements of actual devices and may be useful for calibration of optics-based overlay tools.

Optical characteristics were measured on Spectrophotometer MC-121 (UV-VIS-NIR) by SOL instruments Ltd. with single-beam optical design and dual monochromator. The spectral slit width of the monochromator was fixed and amounted to 2 mm. The spectral scanning step was 2 nm in the range from 190 nm to 1100 nm at an incident angle of 10°. PCs formed on a Si (glass) substrate with a 19 mm diameter were placed in the spectrophotometer experimental chamber. Incidence scheme of an optical beam on the PCs surface is shown in Fig. 1(d). The measurements were carried out only in the reflectant mode.

3. Results and Discussion

SEM images in Figs. 2(a)–2(c) and 3D view in Fig. 2(d) show an anodic film derived from the Al/Ta bilayer on the Si-wafer, after selectively dissolving the porous-alumina. One can see in Figs. 2(a) and 2(b) that the nanocolumns have a fairly typical and uniform nanomorphology, size and hexagonal arrangement. This can be considered a good result, taking into account carrying out the formation without using any methods of increasing nanostructuring and using nanoimprint stamps. However, larger magnification of the SEM image [Fig. 2(c)] displayed fairly significant nanocolumn-free areas of about $122 \times 87\,\mu m^2$, showing uneven arrangement of the columns. This may be either due to the peculiarity of this population formed in tartaric acid 200 V, or due to an error in the anodization technique and poor preparation for SEM. In any case, it can be expected that the nonuniform distribution of the tantalum-oxide nanocolumns will negatively affect the optical characteristics of the nanomaterial.

Figure 3(a) shows the optical reflectant spectrum of the tantalum-oxide nanocolumn sample. Optical absorption is present throughout the ultraviolet range. Approximately at the wavelength of 285 nm, the reflectance begins to grow and reaches its peak at the wavelength of 690 nm. However, the arrangement of the columns is uneven, the reflectant peak centered at about 700 nm is strongly stretched with maximum intensity reaching 28%. At present, a good average result of reflecting PCs on titanium-oxide is 60%[19–26]

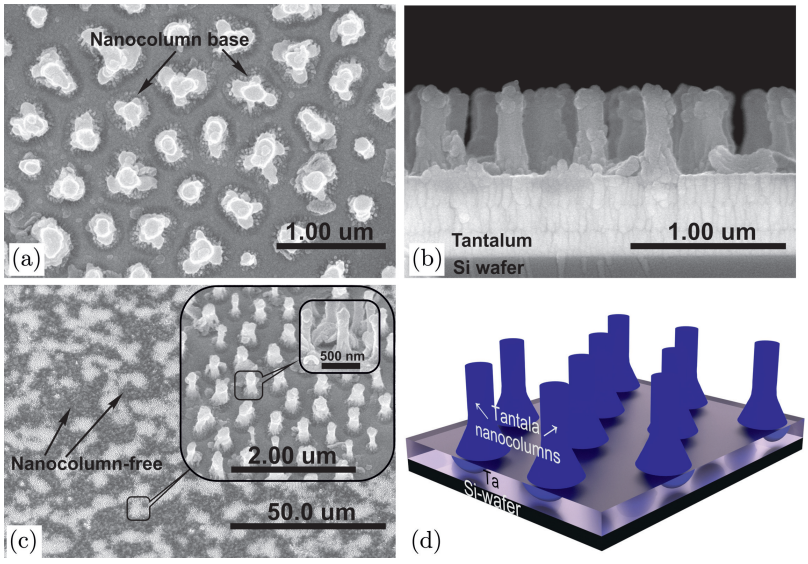

Fig. 2. (a–c) SEM images and (d) schematic 3D view of reflectant PCs formed via porous-alumina-assisted-anodizing bilayer system Al/Ta on Si wafer at 200 V in 0.2 mol · dm^{-3} tartaric acid with subsequent porous-alumina-assisted high-voltage re-anodizing in the mixed solution of 0.5 mol · dm^{-3} boric acid and 0.05 mol · dm^{-3} sodium tetraborate at 400 V. The images demonstrate the samples obtained after the alumina layer dissolution ("alumina-free" samples).

and the value of 85% was reached in Ref. 12. Against this background, the values obtained in this work seem rather modest. Therefore, attempts were made not just to improve the result, but to show that this is fundamentally possible by varying the anodizing conditions. For this, anodizing regimes oxalic acid

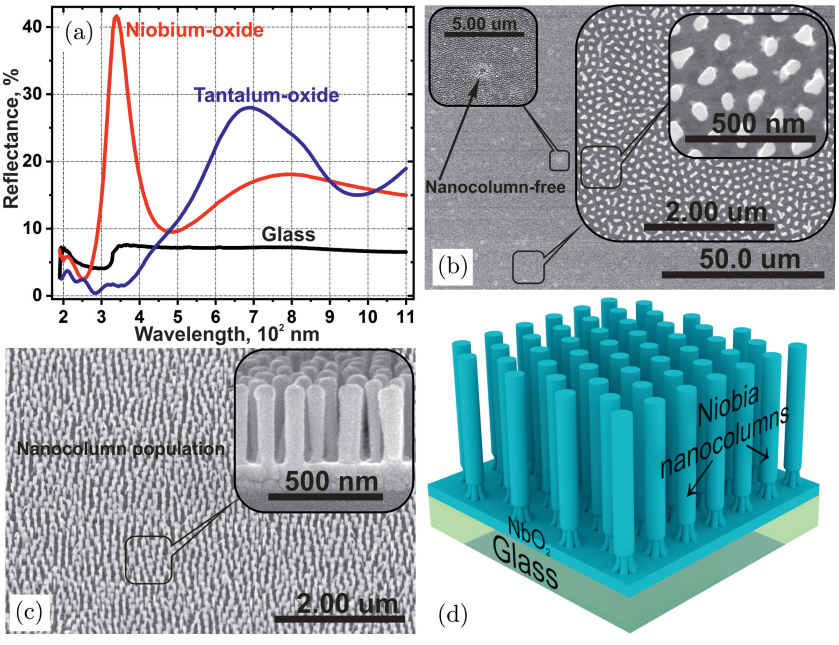

Fig. 3. (a) Optical reflectance of PCs formed via porous-alumina-assisted-anodizing bilayer system Al/Nb and Al/Ta. (b and c) SEM images and (d) schematic 3D view of reflectant PCs formed via porous-alumina-assisted-anodizing bilayer system Al/Nb on glass at 53 V in 0.2 mol · dm^{-3} oxalic acid with subsequent porous-alumina-assisted high-voltage re-anodizing in the mixed solution of 0.5 mol · dm^{-3} boric acid and 0.05 mol · dm^{-3} sodium tetraborate at 230 V. The images demonstrate the samples obtained after the alumina layer dissolution ("alumina-free" samples).

53 V with more reproducible and uniform located nanocolumns were chosen, and the formation was carried out on glass substrates. 53 volts oxalic acid was chosen from the following considerations. Firstly, this mode of anodic alumina formation on a niobium sublayer has been studied in detail and in many ways.[13,27–29] The composition and morphological parameters of niobium-oxide nanocolumns have been established. Secondly, in this mode, the bases of the nanocolumns are combined into a continuous oxide layer due to the small inter-column distance, which does not occur for a tartaric acid solution. Due to this, this mode makes it possible to form an array on the glass surface by completely acidifying the metallic niobium, which is an important aspect for obtaining transparent arrays of nanocolumns. Thirdly, tantalum was replaced by niobium due to better optical characteristics, in particular, higher refractive index and electrophysical properties. In work Ref. 15, it was shown that the niobium-oxide nanocolumns have a semiconducting nature, in contrast to the dielectric nanocolumns of tantalum-oxide,[16] which is of fundamental importance, since it does not allow to completely get rid of the metal due to the interruption of the current supply during the re-anodizing process. Besides, the formation of niobium-oxide nanocolumns in tartaric acid occurs in a goblet-like shape,[13] which reduces their stability and complicates the control of optical reflectance.

SEM surface, cross-section and the schematic 3D view of niobium-oxide nanocolumns are presented in Figs. 3(b)–3(d). The high uniformity of the columns on the surface is confirmed by Fig. 3(b). On the area of $122 \times 87\ \mu m^2$ like tantalum-oxide PC there are no nanocolumn-free areas, only minor point defects present. The surface of Figs. 3(b)–3(c) shows a high reproducibility of the morphological sizes of nanostructures both from column to column and along the column from the continuous oxide layer to the top, which should significantly improve the optical characteristics. Figure 3(a) shows the reflectance of niobium-oxide nanocolumns. Optical absorbance at the level of niobium-oxide nanocolumns on glass substrate is present up to 252 nm in the wavelength, after which it begins to increase sharply to 340 nm where the reflectant level is the maximum value of 42%. The peak is very sharp with the width of 232 nm. Table 1 shows morphological parameter results and optical reflectance of niobium- and tantalum-oxide nanocolumns.

Above all, it should be added that the optical beam falls at an angle of 10° and therefore passes through alternating regions of nanocolumn-air. The number of such layers determines the efficiency of the PC. Therefore, the higher the columns aspect ratio (height/diameter), the more quantity of layers the optical beam will cross and the more efficient the PC will be. The niobium-oxide nanocolumns had a significantly larger aspect ratio of 5.5 than the 3.15 tantalum-oxide nanocolumns, that can be calculated according to the data from Table 1, which explains their greater efficiency. In addition, the efficiency should probably increase with increasing angle of incidence of the optical beam, as in this case the beam must pass through more layers.

Table 1. Morphological, formational and reflectant spectra parameters of PCs produced via porous-alumina-assisted-anodizing of systems Al/Nb and Al/Ta.

Parameters	Tantalum-oxide PCs	Niobium-oxide PCs
Thickness of initial metal, nm	1500/500 (Al/Ta)	1000/50 (Al/Nb)
Column diameters, nm	172	60
Column heights, nm	542	330
Distance between column centers, nm	500	119
Continuous NbO_2 thickness, nm	—	112
Column base diameters, nm	383	—
Re-anodizing voltage, V	400	230
Anodizing voltage, V	200	53
Reflectant maximums (wavelength, nm), %	27.99 (690)	41.63 (340), 18.07 (798)
Reflectant minimums (wavelength, nm), %	0.39 (285), 14.98 (975)	2.51 (252), 9.48 (484)

4. Conclusion

In conclusion, two type PCs with controlled position of the photonic bandgap in the range of 190–1100 nm were synthesized via porous-alumina-assisted-anodizing of systems Al/Nb and Al/Ta. The first type of PCs formed by large tantalum-oxide nanocolumns showed the peak of 28% reflectance at the wavelength of 690 nm. The sufficiently low reflectant value and the large peak width are associated with a nonuniform distribution of nanocolumns on the surface and opaque substrate – Si wafer. The second type of reflectant PCs of smaller morphological sizes was formed from niobium-oxide nanocolumns. The high natural uniformity of the location and morphology of such nanostructures made it possible to achieve the reflectant value of 42% at the wavelength of 340 nm, which is a good initial result and shows significant prospects of such nanostructures for nanophotonics.

Acknowledgment

This work was supported by the State program for scientific research of the Republic of Belarus "Convergence 2025" (tasks 3.03.3 and 2.2.6), "Materials science, new materials and technologies" (task 2.02) and was funded by the Belarusian Republican Foundation for Fundamental Research, grant No. T20PTÈ-006. Andrei Pligovka is grateful to Dr. Gennady Gorokh of BSUIR for sputter-deposition of the Al/Ta bilayers on Si wafer and Al/Nb on glass substrate and Dr. Dmitry Kotov of BSUIR for helping in the UV-VIS-NIR measurements.

References

1. C. A. Jong and T. S. Chin, *Mater. Chem. Phys.* **74** (2002) 201. Doi: 10.1016/S0254-0584(01)00467-9.
2. K. S. Lee, T. M. Lu and X. C. Zhang, *Microelectron. J.* **34** (2003) 63. Doi: 10.1016/S0026-2692(02)00139-8.
3. R. Ab Kadir, R. A. Rani, M. M. Y. A. Alsaif, J. Z. Ou, W. Wlodarski, A. P. O'Mullane and K. Kalantar-Zadeh, *ACS Appl. Mater. Interfaces* **7** (2015) 4751. Doi: 10.1021/am508463g.
4. M.-R. R. Ok, R. Ghosh, M. K. Brennaman, R. Lopez, T. J. Meyer and E. T. Samulski, *ACS Appl. Mater. Interfaces* **5** (2013) 3469. Doi: 10.1021/am400598u.
5. M. R. Ok, R. Ghosh, M. K. Brennaman, R. Lopez, T. J. Meyer and E. T. Samulski, *ACS Appl. Mater. Interfaces* **5** (2013) 3469. Doi: 10.1021/am400598u.
6. U. Huebner, R. Boucher, W. Morgenroth, J. Kunert, H. Roth, H. G. Meyer, T. Glaser and S. Schroeter, *Microelectron. Eng.* **78–79** (2005) 422. Doi: 10.1016/j.mee.2004.12.053.
7. F. Piret, M. Singh, C. G. Takoudis and B. L. Su, *Chem. Phys. Lett.* **453** (2008) 87. Doi: 10.1016/j.cplett.2008.01.021.
8. T. Wahlbrink, J. Bolten, T. Mollenhauer, H. Kurz, K. Baumann, N. Moll, T. Stöferle and R. F. Mahrt, *Microelectron. Eng.* **85** (2008) 1425. Doi: 10.1016/j.mee.2008.01.059.
9. Y. Zhao, X. Zhou, L. Ye, S. Chi and E. Tsang, *Nano Rev.* **3** (2012) 17631. Doi: 10.3402/nano.v3i0.17631.
10. F. Hashemzadeh, R. Rahimi and A. Ghaffarinejad, *Ceram. Int.* **40** (2014) 9817. Doi: 10.1016/j.ceramint.2014.02.072.
11. H. Li, G. Li, J. Zhu and Y. Wan, *J. Mol. Catal. A Chem.* **226** (2005) 93. Doi: 10.1016/j.molcata.2004.09.028.
12. A. I. Sadykov, S. E. Kushnir, N. A. Sapoletova, V. K. Ivanov and K. S. Napolskii, *Scr. Mater.* **178** (2020) 13. Doi: 10.1021/acsami.9b23354.
13. G. G. Gorokh, A. N. Pligovka and A. A. Lozovenko, *Tech. Phys.* **64** (2019) 1657. Doi: 10.1134/S1063784219110124.
14. A. Pligovka, U. Turavets, A. Hoha, S. Zavadski and A. Poznyak, in *Proc. 2020 International Conference Laser Optics (ICLO)*, Vol. 1 (Russia, St. Petersburg, 2020), p. 1. Doi: 10.1109/ICLO48556.2020.9285405.
15. A. Pligovka, A. Lazavenka and G. Gorokh, *IEEE Trans. Nanotechnol.* **18** (2019) 790. Doi: 10.1109/TNANO.2019.2930901.
16. A. N. Pligovka, A. N. Luferov, R. F. Nosik and A. M. Mozalev, *KpbiMuKo 2010 CriMiCo — 2010 20th Int. Crime. Conf. Microw. Telecommun. Technol. Conf. Proc.* (2010), pp. 880–881. Doi: 10.1109/CRMICO.2010.5632734.
17. M. G. Rosenfield, in *Proc. Integrated Circuit Metrology, Inspection, and Process Control VI*, Vol. 1673 (United States, San Jose, 1992), pp. 157–165. Doi: 10.1117/12.59792.
18. M. G. Rosenfield and A. Starikov, *Microelectron. Eng.* **17** (1992) 439. Doi: 10.1016/0167-9317(92)90090-E.
19. L. Zheng, H. Cheng, F. Liang, S. Shu, C. K. Tsang, H. Li, S. T. Lee and Y. Y. Li, *J. Phys. Chem. C* **116** (2012) 5509. Doi: 10.1021/jp212416c.
20. W. T. Kim and W. Y. Choi, *Sens. Actuators A Phys.* **260** (2017) 178. Doi: 10.1016/j.sna.2017.04.039.
21. D. Kim, A. Ghicov, S. P. Albu and P. Schmuki, *J. Am. Chem. Soc.* **130** (2008) 16454. Doi: 10.1021/ja805201v.
22. K. Xie, M. Guo, X. Liu and H. Huang, *J. Power Sources* **293** (2015) 170. Doi: 10.1016/j.jpowsour.2015.05.025.
23. M. Guo, K. Xie, J. Lin, Z. Yong, C. T. Yip, L. Zhou, Y. Wang and H. Huang, *Energy Environ. Sci.* **5** (2012) 9881. Doi: 10.1039/C2EE22854H.

24. J. Lin, K. Liu and X. Chen, *Small* **7** (2011) 1784. Doi: 10.1002/smll.201002098.
25. C. T. Yip, H. Huang, L. Zhou, K. Xie, Y. Wang, T. Feng, J. Li and W. Y. Tam, *Adv. Mater.* **23** (2011) 5624. Doi: 10.1002/adma.201103591.
26. N. A. Sapoletova, S. E. Kushnir and K. S. Napolskii, *Electrochem. Commun.* **91** (2018) 5. Doi: 10.1016/j.elecom.2018.04.018.
27. A. Pligovka, P. Yunin, A. Hoha, S. Korolyov, G. Gorokh and E. Skorokhodov, *Tech. Phys.* **65** (2020) 1771. Doi: 10.1134/S1063784220110213.
28. A. Mozalev, R. M. Vázquez, C. Bittencourt, D. Cossement, F. Gispert-Guirado, E. Llobet and H. Habazaki, *J. Mater. Chem. C* **2** (2014) 4847. Doi: 10.1039/c4tc00349g.
29. A. Mozalev, M. Bendova, R. M. Vazquez, Z. Pytlicek, E. Llobet and J. Hubalek, *Sens. Actuators B Chem.* **229** (2016) 587. Doi: 10.1016/j.snb.2016.02.024.